Remote sensing of mangrove forest phenology and its environmental drivers

Pastor-Guzman, J.[1], Dash, Jadunandan[1*], Atkinson, Peter M.[1,2,3]

[1]Global Environmental Change and Earth Observation Research Group, Geography and Environment, University of Southampton, Southampton SO17 1BJ, UK;
E-Mails: J.Pastor-Guzman@soton.ac.uk (J.P.-G.); pma@lancaster.ac.uk (P.M.A.)

[2]Faculty of Science and Technology, Lancaster University, Lancaster LA1 4YR, UK

[3]School of Geography, Archaeology and Palaeoecology, Queen's University Belfast, Belfast BT7 1NN, Northern Ireland, UK

*Author to whom correspondence should be addressed; E-Mail: J.DASH@soton.ac.uk;
Tel.: +23-8059-7347.

Abstract

Mangrove forest phenology at the regional scale have been poorly investigated and its driving factors remain unclear. Multi-temporal remote sensing represents a key tool to investigate vegetation phenology, particularly in environments with limited accessibility and lack of *in situ* measurements. This paper presents the first characterisation of mangrove forest phenology from the Yucatan Peninsula, south east Mexico. We used 15-year time-series of four vegetation indices (EVI, NDVI, gNDVI and NDWI) derived from MODIS surface reflectance to estimate phenological parameters which were then compared with *in situ* climatic variables, salinity and litterfall. The Discrete Fourier Transform (DFT) was used to smooth the raw data and four phenological parameters were estimated: start of season (SOS), time of maximum greenness (Max Green), end of season (EOS) and length of season (LOS). Litterfall showed a distinct seasonal pattern with higher rates during the end of the dry season and during the wet season. Litterfall was positively correlated with temperature (r=0.88, p<0.01) and salinity (r=0.70, p<0.01). The results revealed that although mangroves are evergreen species the mangrove forest has clear greenness seasonality which is negatively correlated with litterfall and generally lagged behind maximum rainfall. The dates of phenological metrics varied depending on the choice of vegetation indices reflecting the sensitivity of each index to a particular aspect of vegetation growth. NDWI, an index associated to canopy water content and soil moisture had advanced dates of SOS, Max Green and EOS while gNDVI, an index primarily related to canopy chlorophyll content had delayed dates. SOS ranged between day of the year (DOY) 144 (late dry season) and DOY 220 (rainy season) while the EOS occurred between DOY 104 (mid-dry season) to DOY 160 (early rainy season). The length of the growing season ranged between 228 and 264 days. Sites receiving a greater amount of rainfall between January and March showed an advanced SOS and Max Green. This phenological characterisation is useful to understand the mangrove forest dynamics at the landscape scale and to monitor the status of mangrove. In addition the results will serve as a baseline against which to compare future changes in mangrove phenology due to natural or anthropogenic causes.

1. Introduction

Mangroves are a taxonomically diverse assemblage of tree species which have common morphological, biochemical, physiological and reproductive adaptations that allows them to colonise and develop in saline, hypoxic environments (Alongi, 2016). These assemblages form intertidal forests which are one of the most carbon rich ecosystems (Donato et al., 2011) because of their high productivity (Twilley and Day, 1999), rapid sediment accretion (Bouillon et al., 2008) and low respiration rates (Barr et al., 2010). Vegetation phenology, defined as the growing cycle of plants and involving recurring biological events such as leaf unfolding and development, flowering, leaf senescence and litterfall (Njoku, 2014), regulates the timing of plant photosynthetic activity and influences directly the annual vegetation carbon uptake. Vegetation phenology has been a focus of attention in recent years due to a strong and measurable link between biological events and climate (Cleland et al., 2007; Richardson et al., 2013; Dannenberg et al., 2015).

Historically, vegetation phenology was based on field records of key biological events such as budburst, flowering, seed set and leaf senescence (Fitter and Fitter, 2002). Recently, a network of fine-resolution digital cameras installed in the field known as “phenocams”, emerged as a new method to monitor vegetation phenology (Richardson et al., 2007). While this method reduces the subjectivity of human observations, it is limited by its relatively small spatial extent across the globe (Mizunuma et al., 2013; Klosterman et al., 2014). Alternatively, as the reflectance properties of vegetated land varies seasonally in relation to vegetation phenology, the systematic, multi-temporal data collected by optical satellite sensors offer a unique mechanism to monitor vegetation dynamics as this approach allows monitoring of an entire ecosystem rather than individual trees (Reed et al., 2009; White et al., 1997, 1999). This has led to the rise of a new field known as land surface phenology (LSP) (Hanes et al., 2014).

In the last few decades, LSP, which uses time-series of satellite-derived vegetation indices, has received considerable attention given its potential to characterise the interactions between vegetation and climate at broad geographical scales. Pioneer work in the temperate latitudes of the American

continent showed that the start of vegetation greening was controlled by pre-season temperature (White et al., 1997). Moulin et al. (1997) conducted one of the first attempts to map global vegetation phenology using the Advanced Very High Resolution Radiometer (NOAA/AVHRR) at 1º x 1º resolution. The study revealed patterns in the global vegetation phenology related to seasonal variation in climate. For example, the start of vegetation greenness in temperate deciduous forests was strongly influenced by temperature, whereas savannahs were more influenced by rainfall. The capability to study global vegetation dynamics increases as more advanced sensors and new algorithms become available. Zhang et al., (2006) mapped global vegetation phenology at a finer spatial resolution (1 km x 1 km) achieving more realistic results using the Enhanced Vegetation Index (EVI) derived from the Moderate Resolution Imaging Spectroradiometer (MODIS). In the last decade, numerous studies have been carried out to analyse patterns in vegetation phenology at continental and regional scales at a variety of latitudes including the boreal ecosystem (Xu et al., 2013; Jeganathan et al., 2014), Europe (Stöckli and Vidale, 2004; Rodriguez-Galiano et al., 2015a), India (Dash et al., 2010) and the Amazon Forest (Xiao et al., 2005b).

Despite increasing interest in the use of remote sensing to characterise vegetation phenology, most studies of mangrove phenology rely on traditional field methods consisting on *in situ* collection of different components of litterfall (e.g. leaves, branches, flowers and propagules) (Leach and Burgin, 1985). Studies of this nature were documented in mangrove forests across the globe (see Table 1), and those studies have indicated that litterfall dynamics and reproductive phenology of mangroves is driven by a complex interaction of ecological (species composition, competition, reproductive strategy), climatic (air temperature, precipitation, evaporation, hours of sun, wind speed) and local environmental factors (fresh water inputs, tides, flooding, soil salinity, soil nutrients) and natural disturbances (e.g., hurricanes). Moreover, these studies revealed that although mangroves are evergreen species that produce litterfall and replace old leaves continuously throughout the year they generally present a peak of leaf fall, leaf emergence and reproductive structures in the wet season. There are cases, however, where this pattern can be bimodal, with one leaf fall peak in the dry season and one in the wet season.

Although the above studies provide a local perspective of the interaction between mangroves and physical drivers, there are some limitations. For instance, mangroves are often distributed across hundreds of kilometres of coastlines. Thus, spatially restricted studies do not support observation of the phenology phases over the complete extent of the forest. In addition, a common characteristic of those studies is the limited time span, ranging between 1 to 4 years. This relatively short period prevents observing inter-annual variation and trends in phenological metrics and how they are driven by any climatic factors. Spatially continuous and temporally rich information on mangrove phenology would be useful to characterise mangrove forest dynamics at the landscape scale and understand their contribution to biogeochemical cycles.

To date there has been no characterisation of mangrove forests phenology using remote sensing data. In this paper, we estimate and map phenological metrics from time-series of medium resolution satellite sensor imagery in a mangrove forest in the SE of Mexico and investigate their relationship with environmental drivers. The objectives of this research were to (i) estimate phenological parameters using a time-series of MODIS vegetation indices to explore the consistency among them, (ii) map the spatial distribution of phenological metrics (start of growing season, time of maximum greenness, end of growing season and end of season), and (iii) characterise the relationship between phenology dynamics and environmental drivers.

111

112

Table 1. Field studies addressing mangrove forest phenology.

Country	Reference
Australia	Coupland et al., 2005; Duke, 1990
Borneo	Sukardjo et al., 2013
Brazil	Mehlig, 2006; Fernandes, 1999
India	Upadhyay and Mishra, 2010; Wafar et al., 1997
Japan	Kamruzzaman et al., 2016; Sharma et al., 2014
Kenya	Slim et al., 1996
Malaysia	Hoque et al., 2015; Akmar and Juliana, 2012
Mexico	Agraz-Hernández et al., 2011; Utrera-López and Moreno-Casasola, 2008; Aké-Castillo et al., 2006; Arreola-Lizárraga et al., 2004; Day et al., 1987; Lopez-Portillo and Ezcurra, 1985
Panama	Cerón-Souza et al., 2014
South Africa	Rajkaran and Adams, 2007
United States of America	Castañeda-Moya et al., 2013

113

114

115

116

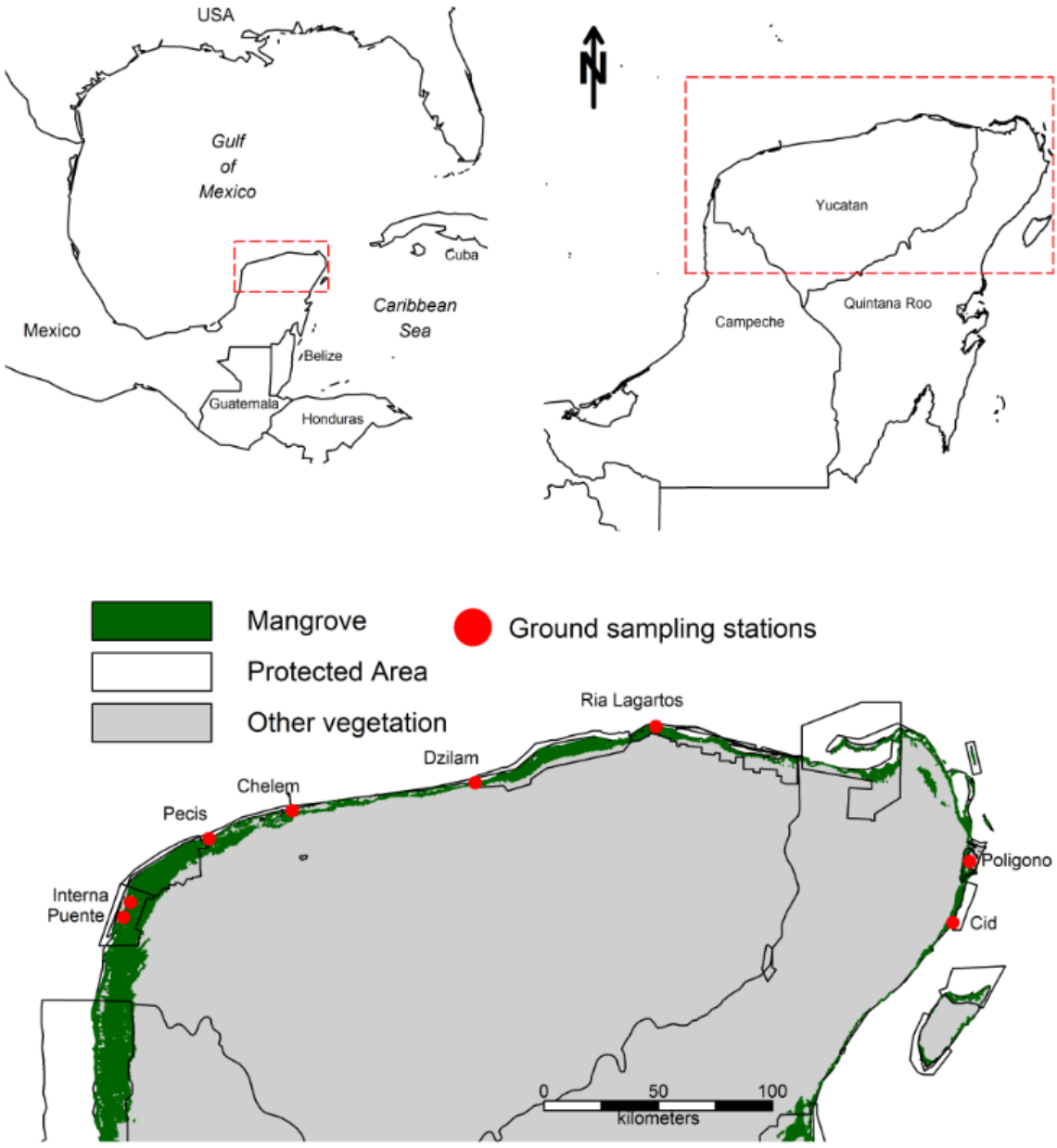

Fig. 1. Study area showing eight ground sampling stations distributed along the Yucatan Peninsula coastline. The figure depicts the spatial distribution of the mangrove forest in green.

2. Methods

2.1. Study area

Yucatan Peninsula is located in SE Mexico (Fig. 1). To the west and north the Yucatan Peninsula is bordered by the Gulf of Mexico and to the east it is bordered by the Caribbean Sea. The area comprises the states of Campeche, Yucatan and Quintana Roo. Except for a narrow fringe of dry climate in the north west (see Fig. S1-S3), the climate of the Yucatan Peninsula is predominantly hot and humid with little precipitation all year and a distinct rainy season in summer (Roger Orellana et al., 2009). The region experiences three seasons: a dry season from March to May, a rainy season from June to October and a cold season from November to February (Herrera-Silveira et al., 1999). The mean annual temperature ranges from 26.5 to 25.5 C and mean annual precipitation ranges from 600 mm to 1100 mm (Roger Orellana et al., 2009). Mangrove forest in the Yucatan Peninsula is found on a flat karstic substrate that facilitates the infiltration of rainfall resulting in the absence of runoff and the lack of important streams above the surface (Pope et al., 1997). The vertical and horizontal range of the tides is variable across the study area as the tide depends on the morphology of a particular location. For the Yucatan Peninsula the tidal range is estimated to be between 0.06 m to 1.5 m (Herrera-Silveira and Morales-Ojeda, 2010). The mangrove forest is separated from the sea by a sand barrier and it extends in a fringe of varying widths parallel to the coast covering an area of approximately 423,751 ha which represents 55% of Mexico's mangrove cover (CONABIO, 2009). Four species of mangrove dominate the landscape: *Rhizophora mangle, Laguncularia racemosa, Avicennia germinans and Conocarpus erectus*. The National Commission for Knowledge and Use of Biodiversity (CONABIO) has a programme for mapping and monitoring mangrove forest based on aerial photography and fine spatial resolution satellite sensor imagery which is updated every five years.

2.2. Data processing

Four major steps were followed in this research as summarized in Fig. 2: (i) remote sensing data pre-processing and computation of vegetation indices, (i) time-series smoothing and estimation of phenological metrics, (iii) *in situ* data collection and comparison of *in situ* data with mangrove phenology.

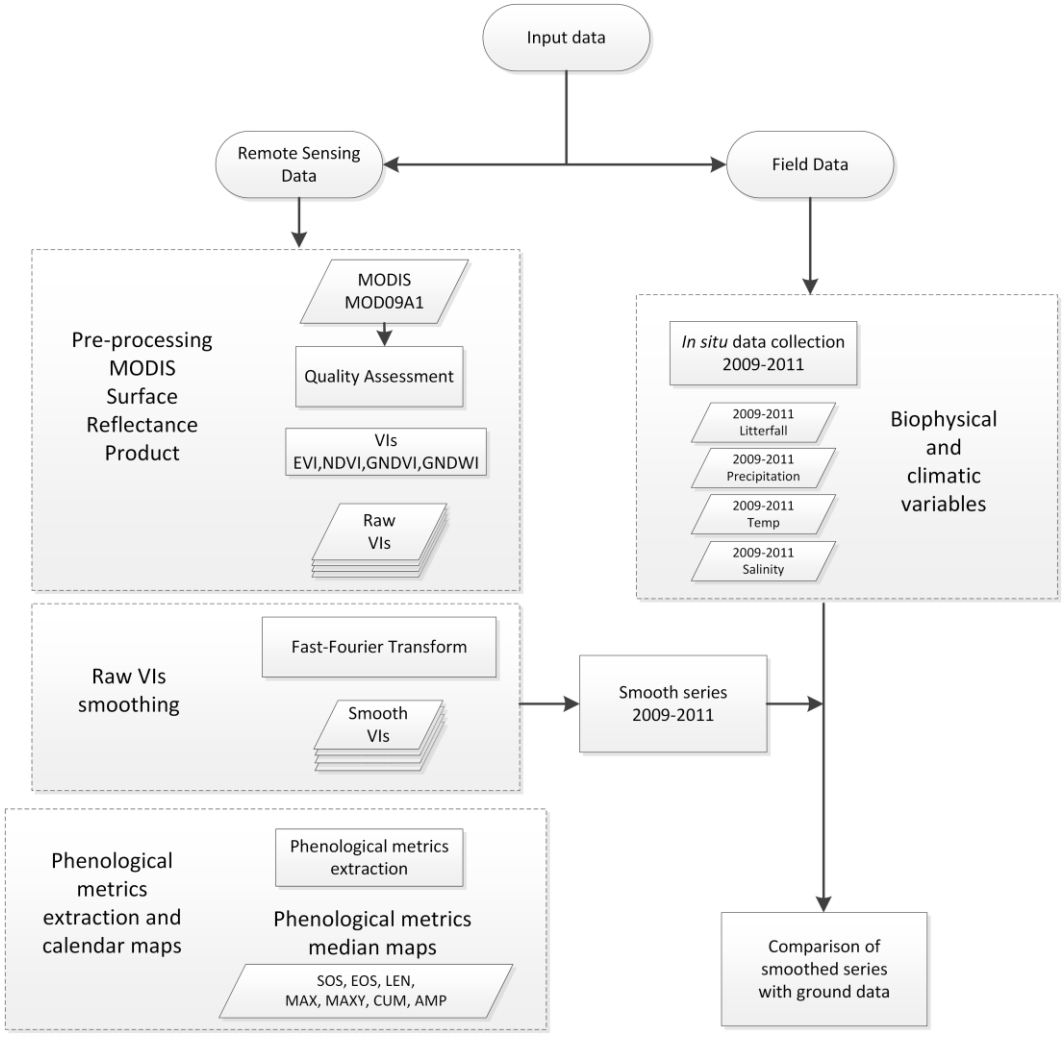

Fig. 2. Schematic diagram illustrating the methodology followed in this research.

Although there is a phenology product readily available it was not used in this research for several reasons. The MODIS Land Cover Dynamics (MCD12Q2) also known as the MODIS phenology product which primarily uses MODIS EVI, offers a global characterisation of vegetation phenology. However, according to the MODIS team the quality assurance layer of this product is not working as intended. In addition, the use of a standard product prevents the computation of other vegetation

indices which can provide complementary information about mangrove forest biophysical variables such as canopy water thickness and chlorophyll content. Further, the use of a standard product limits the user's control over the algorithms for smoothing the time-series and estimating phenology metrics. An exploratory analysis revealed that for the study area, the MCD12Q2 product seems to capture the start of greening season (SOS) at spurious peaks at the first half of the time-series (Fig. S12-S14).

2.2.1. Remote sensing data pre-processing and computation of vegetation indices

To investigate the mangrove phenology this research employed a fifteen-year time-series (2000-2014) of Moderate Resolution Imaging Spectroradiometer (MODIS) land surface reflectance product, 8-day composite MOD09A1 at 500 m spatial resolution, tile h09v06 courtesy of the NASA EOSDIS Land Processes Distributed Active Archive Center (LP DAAC; see https://lpdaac.usgs.gov/). The tiles were reprojected using the MODIS Reprojection Tool. In addition, quality assessment (QA) was applied to each pixel using the 32-bit QA band. Only those pixels that met the following criteria were included in the analysis: MODLAND QA produced at ideal quality, the highest data quality for all reflectance bands, atmospheric and adjacency correction performed.

Vegetation indices have been demonstrated to be a useful tool in assessing vegetation biophysical variables. Therefore, in this research four vegetation indices were used to investigate mangrove biophysical variables and to track their seasonality. The indices used were: Normalized Difference Vegetation Index (NDVI), Enhanced Vegetation Index (EVI), Green Normalized Vegetation Index (gNDVI) and Normalized Difference Water Index (NDWI). The NDVI is perhaps the most widely employed index in vegetation phenology (Adole et al., 2016; Julien and Sobrino, 2009), which allows comparison with previous studies. Although NDVI is used widely it tends to saturate at high biomass or at high chlorophyll concentration, which is especially likely for mangroves, and it is affected by soil background, atmospheric effects and aerosols. EVI has an improved sensitivity to high biomass while it compensates for soil background and atmospheric effects using the canopy background adjustment (L=1), the coefficients of aerosol resistance (C_1=6, C_2=7.5) and the gain factor (G=2.5) (Huete et al., 2002). gNDVI uses the green band of MODIS and has been more directly related to leaf

chlorophyll concentration (Gitelson et al., 1996). NDWI is less sensitive than NDVI to atmospheric scattering and is related to vegetation moisture content (Gao, 1996). The indices are computed as follows:

$$EVI = G * \frac{NIR - Red}{NIR + C1 * Red - C2 * Blue + L} \quad \text{Eq. (1)}$$

$$NDVI = \frac{NIR - Red}{NIR + Red} \quad \text{Eq. (2)}$$

$$gNDVI = \frac{NIR - Green}{NIR + Green} \quad \text{Eq. (3)}$$

$$NDWI = \frac{NIR - SWIR}{NIR + SWIR} \quad \text{Eq. (4)}$$

For MOD09A1 data, band 1 corresponds to the reflectance in the red region of the spectrum (620-670 nm), band 2 represents the near infrared reflectance (871-876 nm), band 3 represents the blue region of the spectrum (459-479 nm) and bands 4 and 5 correspond to the green (545-555 nm) and SWIR (1230-1250) regions, respectively (see documentation at https://lpdaac.usgs.gov). In addition, non-mangrove pixels were masked out using the mangrove distribution shapefile generated by the National Commission for Knowledge and Use of Biodiversity (CONABIO, 2013). The dataset was produced using SPOT-5 imagery from 2010 with a spatial resolution of 10 m. Further, only MODIS pixels that had more than 60% mangrove cover were used in the analyses.

2.2.2. Time-series smoothing and phenological metrics estimation

Time-series smoothing

Time-series of remote sensing data contain noise due to atmospheric conditions, aerosols and clouds at the time of data acquisition. Therefore, it is necessary to remove this contamination by using curve fitting methods which smooth the data and estimate the underlying signal prior to estimating phenological metrics. Several smoothing methods are used commonly ranging from relatively simple techniques such as the median filter (Reed et al., 1994) or moving averages to more complex algorithms including the Savitzty-Golay, Asymmetric Gaussian, Double Logistic and Discrete Fourier Transform (DFT) methods (Jonsson and Eklundh, 2002; Zhang et al., 2003; Atkinson et al., 2012). The DFT algorithm was selected to decompose the mangrove signal because it has consistently produced smaller root mean square error (RMSE) between the input and fitted data over a variety of

vegetation types including evergreen vegetation (Atkinson et al., 2012). The principle behind DFT is that any complex vegetation growth cycle can be decomposed into a series of sinusoids of different frequencies and a constant (Jakubauskas et al., 2001; Wagenseil and Samimi, 2006; Atkinson et al., 2012). The sinusoids with their frequencies (harmonics) are then summed through a process known as Inverse Fourier Transformation to form a complex smooth wave that resembles the original input profile with the high frequency noise removed. The Inverse Fourier Transform has the advantage of requiring minimum user input (it only needs the user to decide the number of harmonics to reconstruct the profile). This technique has been used widely to smooth time-series of satellite sensor data covering a wide range of environments (Roerink et al., 2000; Jakubauskas et al., 2001; Moody and Johnson, 2001; Dash et al., 2010; Jeganathan et al., 2010a, 2010b; Atkinson et al., 2012; V. Rodriguez-Galiano et al., 2015ab). Typically one to five harmonics are recommended to efficiently reconstruct the natural annual phenological profile (Geerken, 2009). An exploratory analysis revealed that the first four harmonics plus the mean satisfactorily reconstructed the phenological profile (Fig. S11-S14); therefore, four harmonics plus the mean were used in in this research. Prior to reconstructing the time-series with DFT, obvious dropouts from the raw input time-series are removed. Then, the removed dropout is replaced by a moving average which considers valid neighbouring values; in this way the new interpolated value preserves the trend of its temporal neighbours. There is a limit for the number of missing values that are interpolated. If there is more than a month of consecutive missing values the time-series is discarded and no phenological metrics are estimated.

Phenological metrics estimation

Data processing, DFT based smoothing and phenological metrics estimation based on Dash et al. (2010) and Atkinson et al. (2012) were developed and implemented in the R Programming Language (R Core Team, 2015).

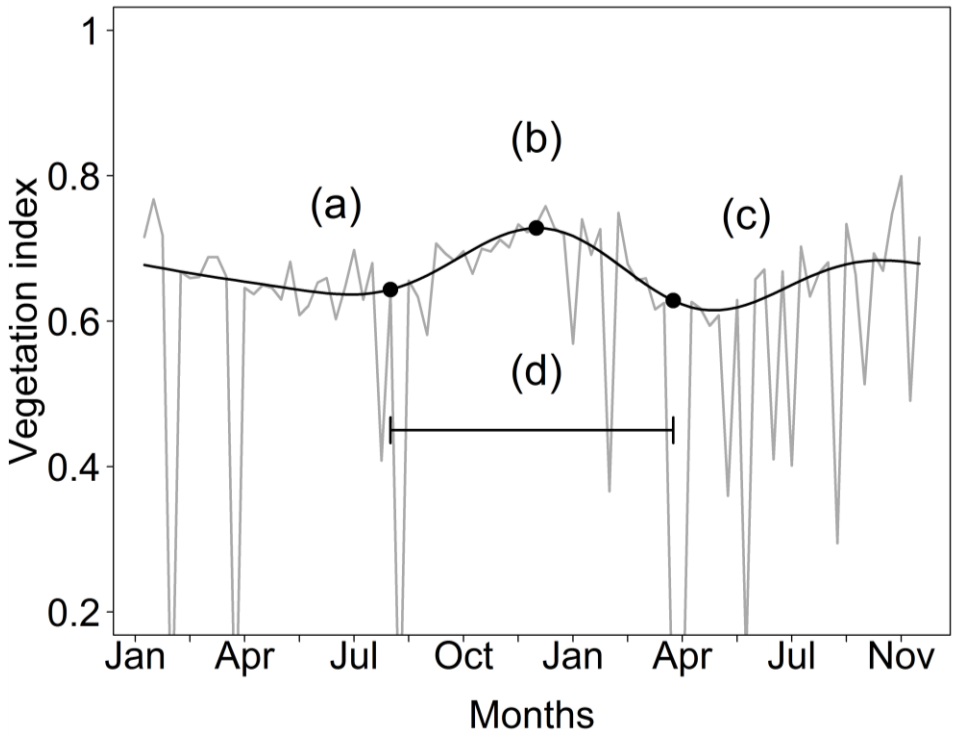

Fig. 3. Graphical illustration of phenological metrics estimation using DFT and inflection point algorithms: (a) start of green up season (SOS), (b) time of maximum greenness (Max Green), (c) end of growing season (EOS) and (d) length of growing season (LOS). Grey solid line represents a raw data pixel profile and the black solid line represents the smoothed series using four harmonics plus the mean. The pixel profile was extracted from the season 2010-2011 at the coordinates 20.66601 N, -90.35937 W.

The 15-year time-series was divided into 14 seasons. For each season four phenological metrics were estimated: start of growing season (SOS), end of growing season (EOS), length of season (LOS), time of maximum vegetation greenness (Max Green) (Fig. 3). Several methods are used to estimate phenological metrics from smooth pixel profiles such as threshold based, trend derivative methods and inflection point methods (Reed et al., 1994; Jönsson and Eklundh, 2002, 2004; Dash et al., 2010). In this research, the inflection point method was adopted because it does not assume a pre-defined value as transition date and it is easy to implement. The SOS was defined as the valley point at the start of the increasing trend in the vegetation index values before the first half of the smooth curve, while the EOS was defined as the valley point at the end of the decreasing trend in the vegetation index values after the first half of the curve (Fig. 3). The process consists of extracting the dominant peak (Max Green) in the curve and iterating backwards and forward to find the SOS and EOS (see Dash et al., 2010 for more detail); LOS was defined as the difference between EOS and SOS. Finally, the phenology characterisation maps were created by computing the median from the 14 seasons.

2.2.3. *In situ* data collection and comparison of *in situ* data with mangrove phenology

In situ data collection

This research used data produced by the regional programme for characterisation and monitoring of mangrove ecosystems in the Gulf of Mexico and Mexican Caribbean: Yucatan Peninsula (Herrera-Silveira et al., 2014). A field campaign was conducted from January 2009 to October 2011 in 16 sites located along the coast of Yucatan Peninsula within MODIS tile h09v06 (Fig. 1, Table S1). The objective was to characterise, and to establish a baseline for monitoring, the mangrove forest of the region (Herrera-Silveira et al., 2014). The monitoring involved monthly *in situ* measurements of interstitial salinity and litterfall. Rainfall and temperature data were obtained from automatic meteorological stations. In this research, only those sites with meteorological data (Table S1) were used in the analysis because one the main objectives was to examine the link between climatic variables and mangrove forest phenology. The fieldwork was conducted by the Centre of Research and Advanced Studies (CINVESTAV) campus Merida, Yucatan and it was funded by the National Commission for the Knowledge and Use of Biodiversity (CONABIO). Two permanent sampling plots of 10 m by 10 m were established at each site. Five litterfall traps were located at each sampling plot

306 at 1.3 m height from the ground. The vegetative material was collected monthly. It was then
307 dehydrated for 72 hours and litterfall components were separated. Dry litterfall was weighed and
308 represented in grams per square metre per month. Temperature and rainfall data were collected from
309 automatic meteorological stations located at the nearest town. The stations recorded the mean of the
310 meteorological variables every 10 minutes and were expressed as monthly means. Monthly
311 measurements of interstitial water salinity were conducted at each site using a YSI-30 multiprobe
312 sensor (YSI, Xylem Inc., Yellow Springs, Ohio, U.S.A.); the water was sampled at 30 cm depth and
313 expressed in grams per kilogram.
314 *Comparison of in situ data with mangrove phenology*
315 The *in situ* data described above were used for two purposes. First, litterfall was employed to validate
316 the mangrove phenology information derived from satellite sensor data. Second, physical variables
317 (rainfall, temperature and salinity) were used to identify the factors driving mangrove phenology.
318 Spearman's rank correlation analysis was conducted between VIs, litterfall, rainfall, temperature
319 using the monthly mean of all sites to explore the relationships between climatic variables and
320 mangrove greenness and between climatic variables and litterfall. In addition, Spearman's rank
321 correlation analysis was carried out to examine the relationship between cumulative rainfall and
322 phenological metrics SOS, Max Green across sites (eight sites) and years (2009 to 2011) to assess the
323 influence of climatic variables on the main phenological events in the mangrove forest. Spearman's
324 rank correlation was used because normality in the data and a linear relationship could not be assumed
325 in all cases and because building a predictive model was beyond the scope of the analysis. Data
326 analysis was carried out in R (R Core Team, 2015).
327
328 **3. Results**
329 3.1. Relationship between litterfall, physical variables and vegetation indices temporal profiles
330 Fig. 4 shows the seasonal variation profiles of monthly litterfall, soil interstitial salinity, temperature,
331 rainfall and vegetation indices at one representative ground sampling station located in the north west
332 of Yucatan Peninsula from January 2009 to October 2011. At this site, during the *in situ* data
333 collection period air temperature increased from March to August with a concomitant increase in

salinity. From January to May rainfall remained below 50 mm. Moreover, an increment in rainfall appears to be followed by a decrease in salinity. This seasonal pattern seems to be consistent across all sampling sites (Fig. S4-S10).

3.1.1. Litterfall and physical variables

Litterfall production is continuous throughout the year in the mangrove forest of Yucatan Peninsula. Minimum values of litterfall were recorded between December and February during the cold season. Two peaks in litterfall were observed, one between April and June and the second between August and October. The first peak in litterfall corresponds to the end of dry season and beginning of rainy season while the second peak corresponds to the late rainy season (Fig. 4a). Both peaks are composed of leaves, stems and reproductive structures, but reproductive structures are more common in the second litterfall peak. A large positive correlation (r=0.88, p<0.01) was observed between litterfall and temperature, a moderate significant positive correlation (r=0.70, p<0.01) was observed between litterfall and salinity while a weak and not significant correlation (r=0.25, p>0.1) was observed between litterfall and rainfall.

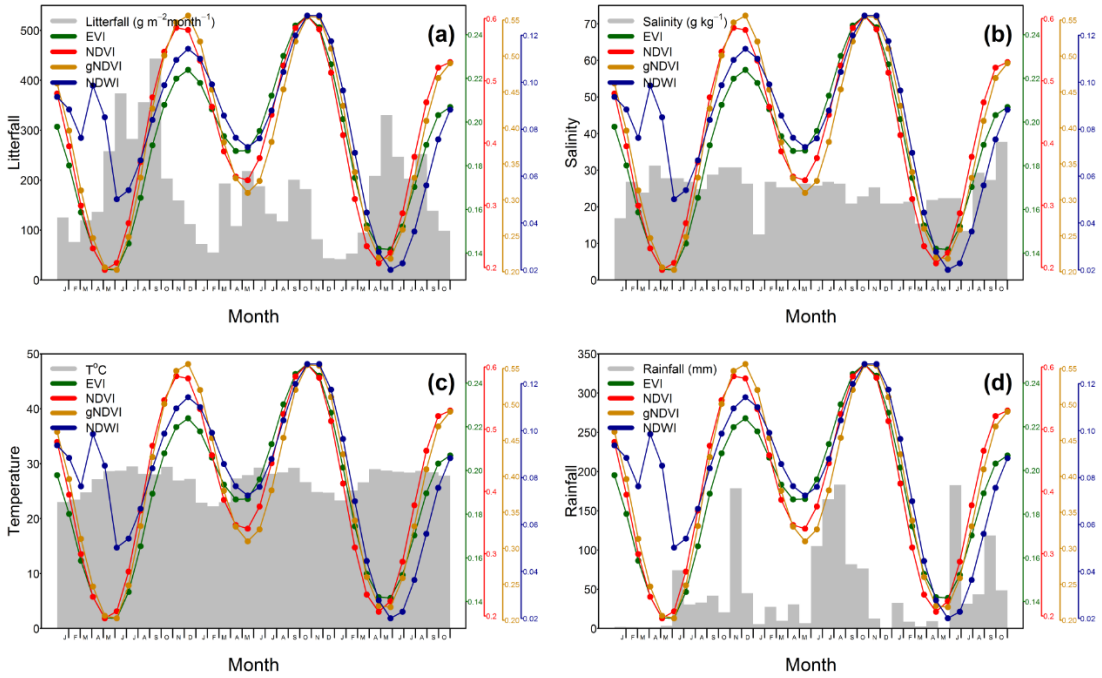

Fig. 4. Seasonal variation in vegetation indices, litterfall (a), salinity (b), temperature (c) and rainfall (d) at the ground station Interna located in the north west of the Yucatan Peninsula between January 2009 and October 2011.

3.1.2. Litterfall and vegetation indices profiles

In Fig. 4, the vegetation indices profiles were averaged monthly to match the temporal resolution of the litterfall data. The temporal pattern of vegetation indices shows that the seasonality of mangrove forest growth is unimodal in nature, it presents a continuous decrease from January to March 2009, reaching a minimum between April and June; then vegetation indices increase steadily from July to September. Mangrove greenness had broadly a negative correlation with litterfall; periods of minimum greenness were coincident with maximum litterfall, and significant negative correlations were observed for gNDVI (p<0.05) (Fig. 5). Further, mangrove greenness appears to lag behind the second peak of litterfall by two to three months. The vegetation indices seasonal pattern described is consistent across all sampling sites (Fig. S4-S10).

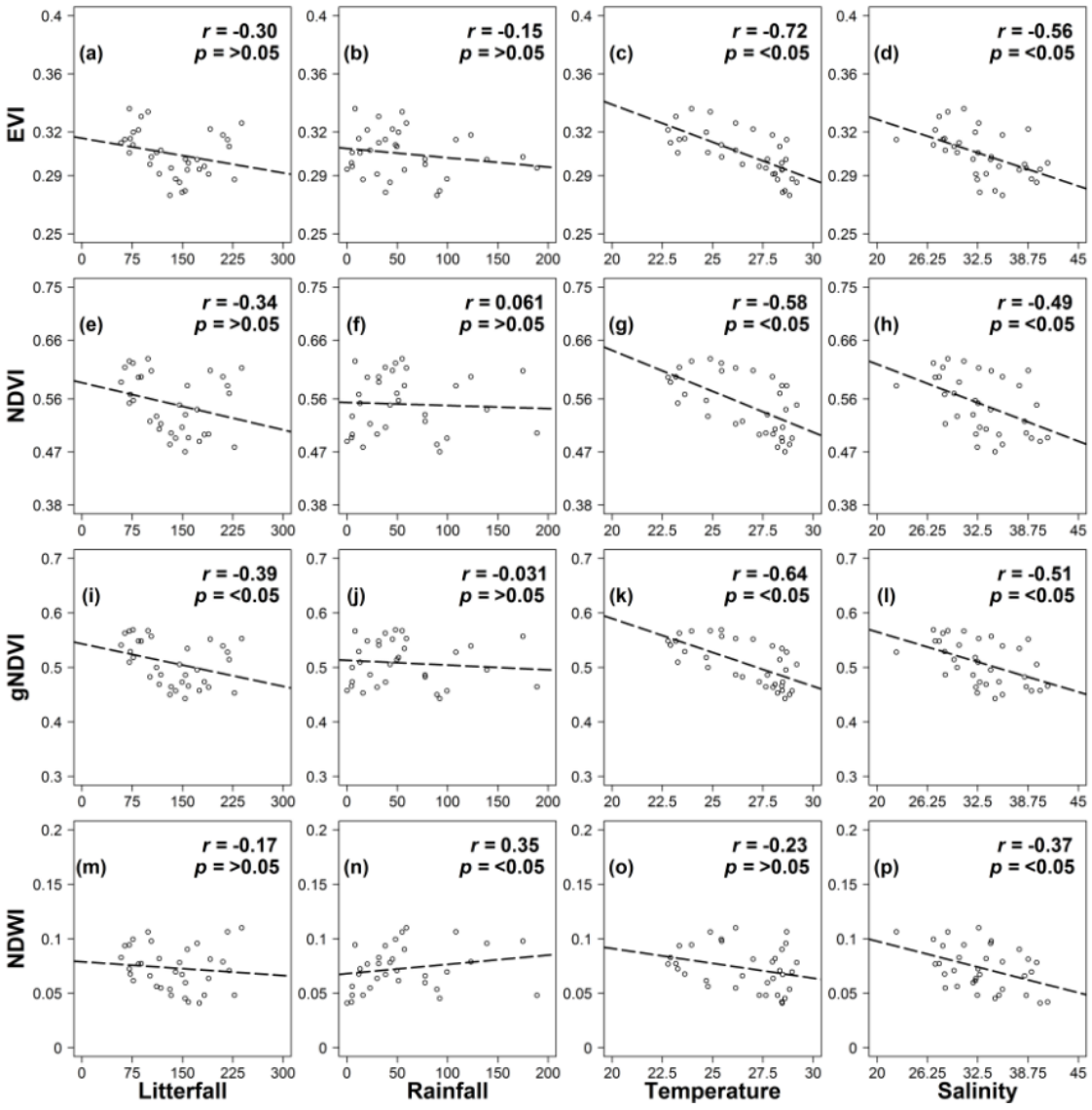

Fig. 5. Scatterplots describing the relationship between monthly vegetation indices values and monthly values of four physical *in situ* variables: litterfall, rainfall, temperature and salinity from January 2009 to October 2011 (n=34). Dominant correlations are observed for EVI, gNDVI and NDVI.

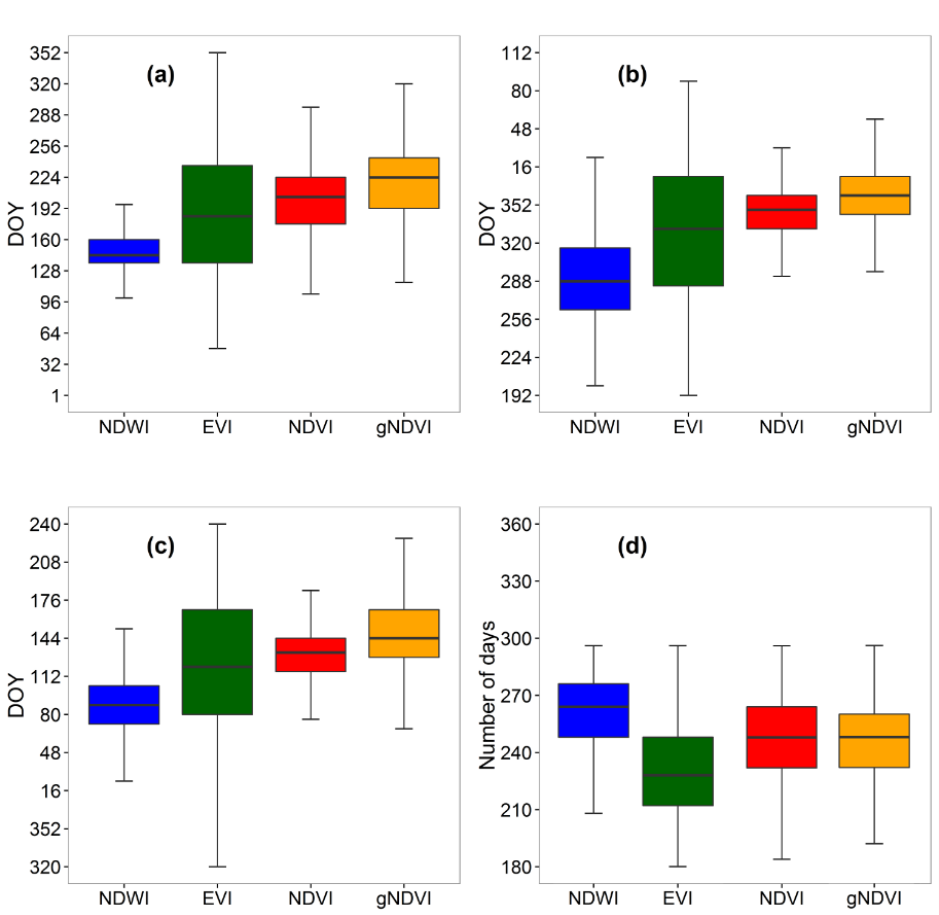

Fig. 6. Distribution of phenological metrics for the mangrove forest of Yucatan Peninsula. The green, red, orange and blue boxes denote EVI, NDVI, gNDVI and NDWI, respectively. The boxplots are ordered from earlier to later dates (or minimum to maximum, depending on the phenological metric). The letters on the plots denote the phenological metrics as follows: (a) SOS, (b) Max Green, (c) EOS and (d) LOS. The middle line of the box represents the median, the lower and upper boundaries of the box are located at the first and third quartile, respectively, and the bars indicate maximum and minimum values.

In general, the temporal profiles of the four vegetation indices were negatively correlated with the physical variables (Fig. 5). Temperature and salinity were significant for NDVI, EVI and gNDVI (p<0.05). Maximum NDVI, EVI and gNDVI seem to lag behind maximum rainfall by two to three months (Fig. 4; Fig. S4-S10). NDWI and rainfall have a weak, positive, but not significant correlation.

3.2. Regional mangrove phenology

Fig. 6 illustrates the distribution of the median of the phenological variables derived from the calendar maps. To examine the spatial distribution of the phenological variables, calendar maps of SOS, Max Green, EOS and LOS were created by computing the median from the 14 seasons. For brevity, only the EVI phenological maps are presented in the main paper (Fig. 7-10) and the maps for NDVI, gNDVI and NDWI are presented as supplementary figures (Fig. S15-S26).

The dates of phenological variables depend upon the choice of VI. Overall, the timing of SOS, Green Max and EOS is reached first by NDWI, next by EVI, then by NDVI and finally by gNDVI (Fig. 6a-c). SOS occurred at DOY 144 (third week of May), DOY 184 (July), DOY 200 (mid-July) and DOY 220 (August) for NDWI, EVI, NDVI and gNDVI, respectively.

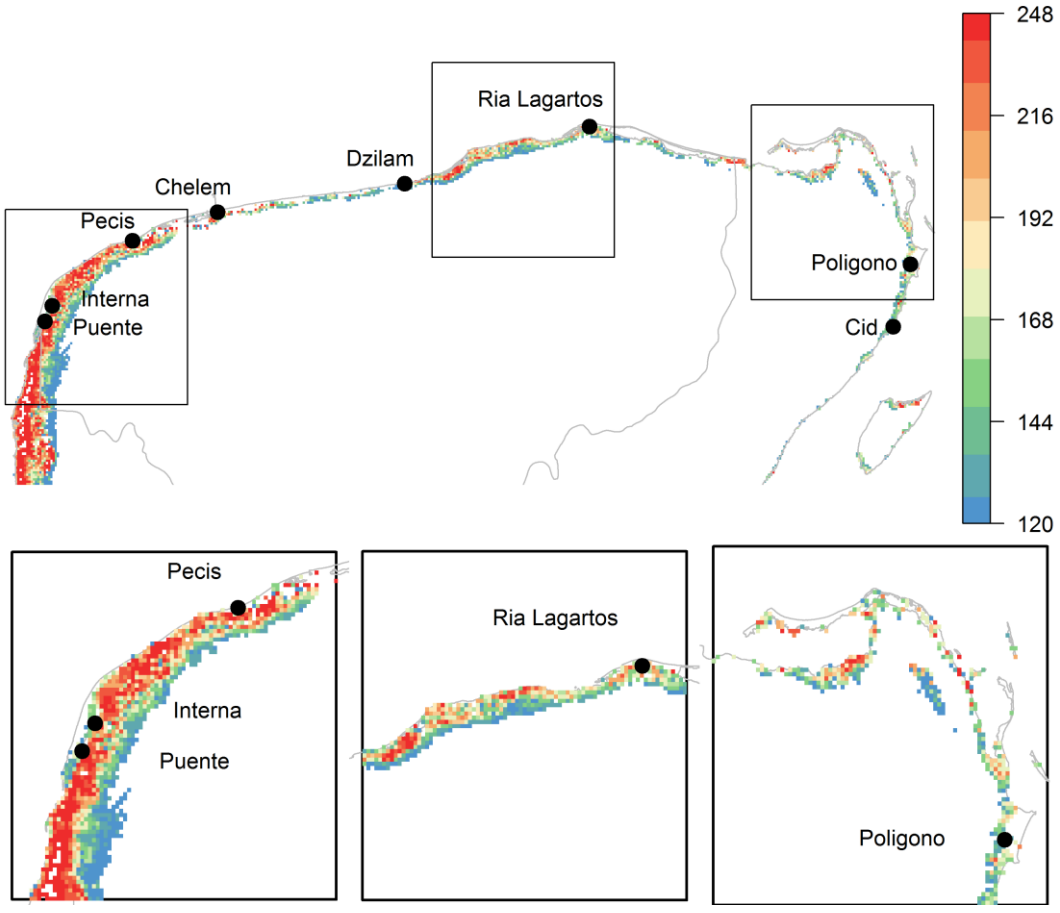

Fig. 7. Spatial distribution of EVI SOS in the mangrove forest of Yucatan Peninsula. The map shows the integrated median for the period 2000-2014. The top figure is a map of the entire study area, while at the bottom, from left to right, the figure shows a zoom of the west,

north and north-east of the Yucatan Peninsula. The continuous colour ramp on the left indicates the DOY of SOS, with earlier SOS in blue and later SOS in yellow and red. Non-mangrove pixels were masked out using the land cover map of the Yucatan Peninsula (CONABIO, 2013)

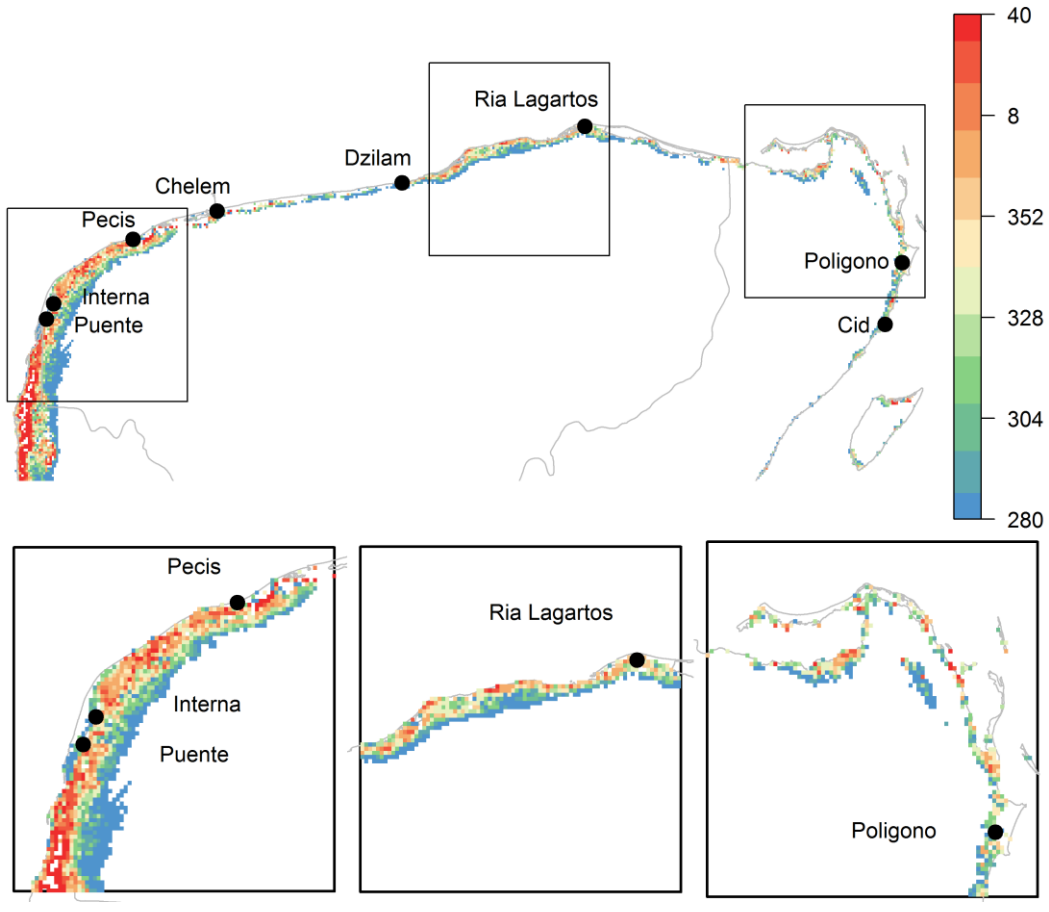

Fig. 8. Spatial distribution of time of EVI maximum greenness (Max Green) in the mangrove forest of Yucatan Peninsula. The map shows the integrated median for the period 2000-2014. The top figure is a map of the entire study area, while at the bottom, from left to right, the figure shows a zoom of the west, north and north-east of the Yucatan Peninsula. The continuous colour ramp on the left indicates the DOY of Max Green, with earlier Max Green in blue and later Max Green in yellow and red.

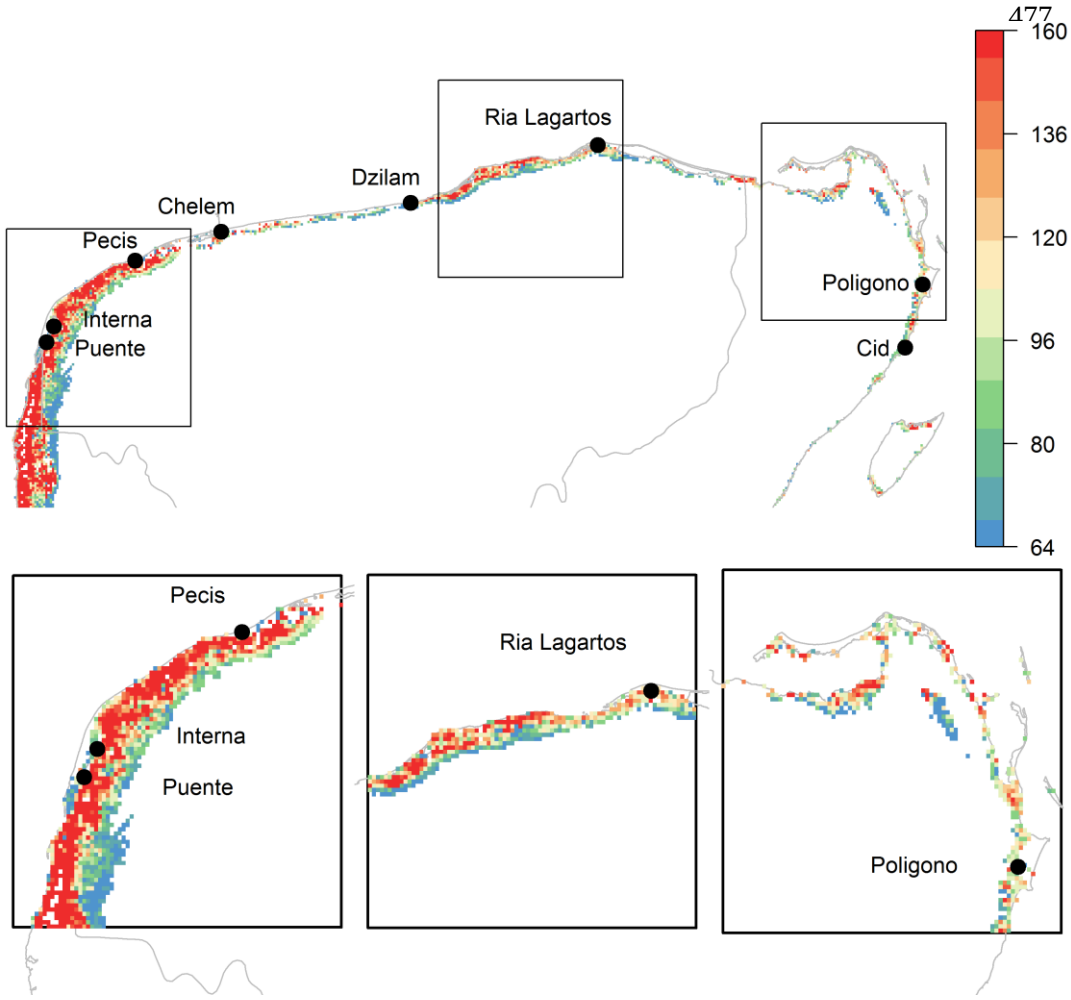

Fig. 9. Spatial distribution of time of EVI EOS in the mangrove forest of Yucatan Peninsula. The map shows the integrated median for the period 2000-2014. The top figure is a map of the entire study area, while at the bottom, from left to right, the figure shows a zoom of the west, north and north-east of the Yucatan Peninsula. The continuous colour ramp on the left indicates the DOY of EOS, with earlier EOS in blue and later EOS in yellow and red.

Spatially, EVI SOS of the mangrove forest of Yucatan Peninsula is reached first in the east of the peninsula and later in the north and the west (Fig. 7). A notable feature particularly in the north and west of the peninsula is the earlier SOS dates at the edge of the mangrove forest and later dates at the interior.

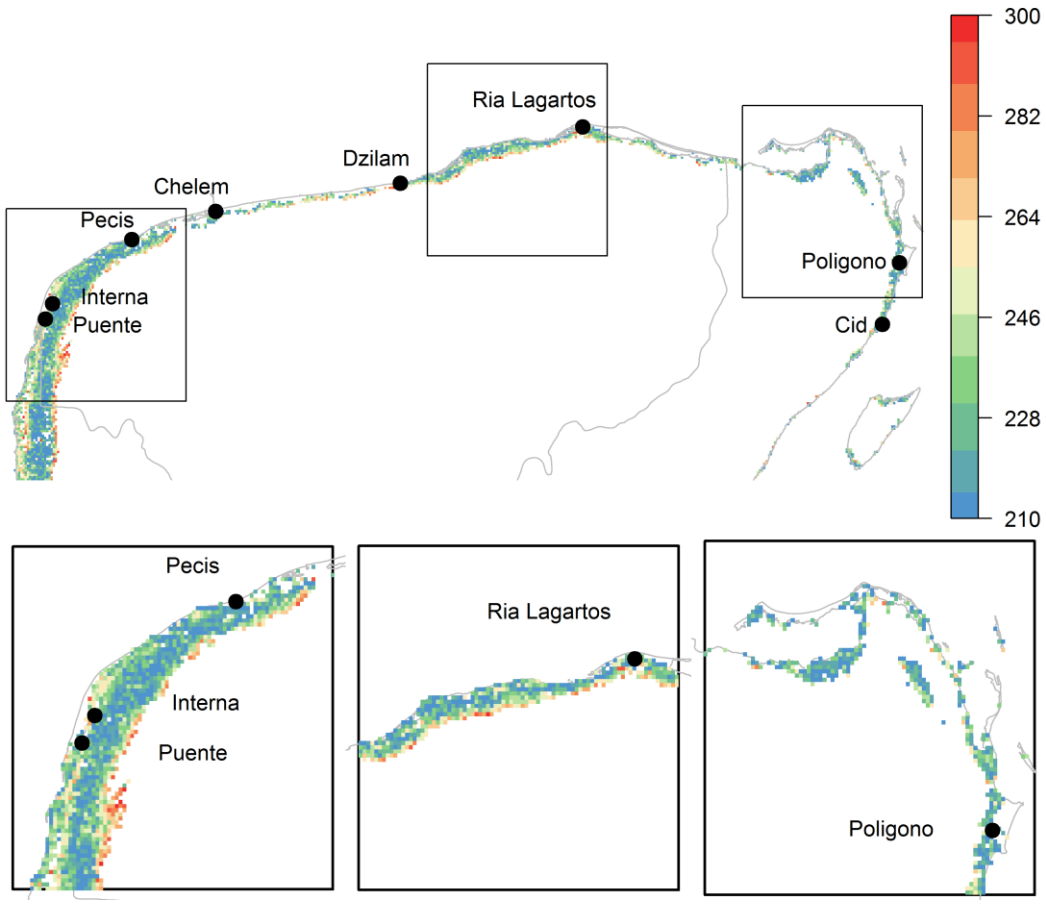

Fig. 10. Spatial distribution of time of EVI LOS in the mangrove forest of Yucatan Peninsula. The map shows the integrated median for the period 2000-2014. The top figure is a map of the entire study area, while at the bottom, from left to right, the figure shows a zoom of the west, north and north-east of the Yucatan Peninsula. The continuous colour ramp on the left indicates number of days, shorter LOS in blue and longer LOS in yellow and red.

Max Green was estimated at DOY 288 (mid-October) for NDWI, at DOY 332 (end of November) for EVI, at DOY 348 (mid-December) for NDVI and at DOY 360 (end of December-beginning of January) for gNDVI (Fig. 6b). EOS occurred at DOY (104) for NDWI, at DOY (136) for EVI, at DOY (148) for NDVI and at DOY (160) for gNDVI (Fig. 6c). The spatial distribution of NDVI Max Green and EOS is generally similar to that of the SOS. That is, delayed Max Green and EOS dates are coincident with delayed dates of SOS (Fig. 8-9; Fig. S15-S23). The mangrove LOS duration ranged between 228 to 264 days; shorter for EVI and longer for NDWI (Fig. 6d). The NDVI LOS was

homogeneous across the study area; longer EVI LOS durations were observed in the north or north west of the peninsula (Fig. 10).

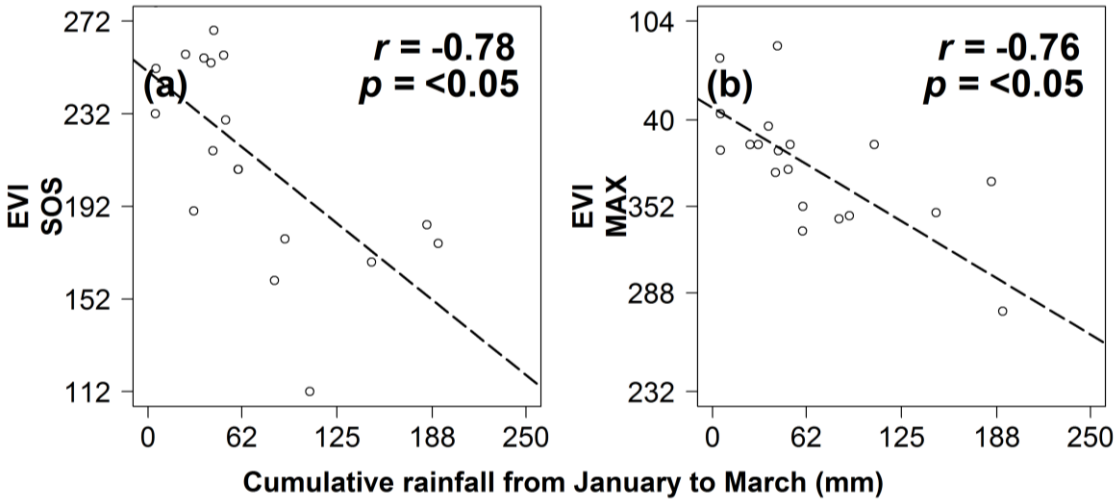

Fig. 11. Relationship between cumulative rainfall and mangrove forest phenological variables. The scatterplots describe the relationship between EVI SOS and MAX with the accumulated rainfall (mm) between January and March. The scatterplots suggest that an increase in rainfall during the first three months of the year leads to an earlier maximum greenness.

3.3. Relationship between satellite-derived phenology and rainfall

To investigate the relationships between the mangrove forest phenological variables and physical drivers, correlation analysis was conducted between the timing of phenological variables and the cumulative temperature, rainfall and salinity. Correlations were weak and not significant for temperature and salinity (results not shown); however, cumulative rainfall from January to March produced a large negative correlation ($r > -75$, $p < 0.05$) with the timing of EVI SOS and Max Green (Fig. 11) and this pattern was also shown by the other three vegetation indices (Fig. S27). Further analysis was carried out to examine if the effect of rainfall on the phenological variables observed using *in situ* data was consistent using rainfall gridded data. Fig. 12 shows the relationship between EVI SOS and cumulative

549 (January to March) rainfall using CHIRPS gridded data for 2009 to 2011 at 0.05 º spatial
550 resolution. The figure confirms the negative correlation between the cumulative precipitation
551 and EVI SOS across the Yucatan Peninsula. Overall, this pattern was consistent across
552 seasons (Fig. S28).
553
554
555
556
557
558
559
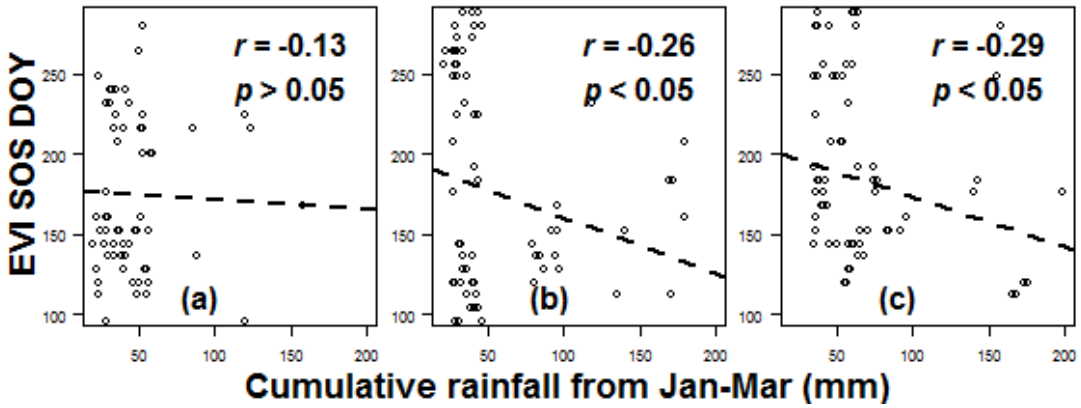

560 Fig. 12. Panels a, b and c represent the Spearman correlation between cumulative rainfall
561 from January to March and the timing of EVI start of greening season (SOS) for 2009, 2010
562 and 2010, respectively. Rainfall corresponds to Climate Hazards Group InfraRed
563 Precipitation with Station data (CHIRPS) gridded data at 0.05 º. Correlations were calculated
564 using pixels with mangrove cover greater than 30% for each CHIRPS rainfall pixel.
565
566
567
568
569
570
571
572
573

4. Discussion

In this paper, 15 years of 8-day MODIS composites were used to characterise the phenology of the mangrove forest of Yucatan Peninsula, SE Mexico. The present study used four vegetation indices, EVI, NDVI, gNDVI and NDWI computed from the MODIS surface reflectance product to derive the SOS, Max Green, EOS and LOS of the mangrove forest. The vegetation indices temporal profiles suggest that although mangrove is an evergreen forest it exhibits seasonal variation in greenness detectable using moderate spatial resolution (500 m) remotely sensed data. *In situ* data on litterfall, temperature, precipitation and salinity were used as possible explanatory drivers of the mangrove forest phenology. To our knowledge, this is the first attempt to provide a regional scale characterisation of the main phenological events of a mangrove forest and assess its relationship with physical drivers and litterfall.

Mangrove litterfall is commonly used as an indicator of forest productivity. Attempts to understand the drivers of mangrove forest litterfall dynamics have tried to establish correlations with physical variables such as wind speed, temperature, rainfall, evaporation and hours of sunshine, but given the disparity in results it is difficult to generalize conclusions. In our study, temperature and salinity were linearly correlated with litterfall. The dynamics of litterfall in the Yucatan Peninsula was in agreement with reports from the Gulf of Mexico (Gill and Tomlinson, 1971; Day et al., 1987; Day Jr. et al., 1996; Utrera-López and Moreno-Casasola, 2008) and previous records in the study area (Zaldivar-Jimenez et al., 2004). These studies have reported continuous litterfall throughout the year with leaf litter the main component, low litterfall values during the cold season, a peak in litter at the end of the dry season and most of the litterfall occurring in the rainy season with a higher proportion of reproductive structures. The pattern described responds to environmental adaptations. On the one hand, during periods of water stress characterised by increases in evapotranspiration and soil salinity due to higher temperatures or decreases in soil moisture due to lack of precipitation and low tides, mangrove trees shed leaves, potentially with a decrease in leaf cover (Medina, 1999). Leaf shedding in mangroves has been widely cited as an adaptation to saline environments (Hasegawa et al., 2000),

more specifically as a mechanism to eliminate salt from the tissue (Tomlinson, 1995; Zheng et al., 1999). Further, the physiological stress caused by high pool water salinity has been related to reductions in photosynthetic radiation-use-efficiency (Barr et al., 2013; Song et al., 2011). On the other hand, during the wet season litterfall contains a higher proportion of flowers, fruits and seedlings. Fresh water input from rainfall leads to higher water levels and milder salinity, and these conditions favour the dispersal of seedlings (Lopez-Portillo and Ezcurra, 1985).

In other tropical evergreen and deciduous forests canopy seasonality is regulated by rainfall seasonality (Chave et al., 2010; Zhang et al., 2014) but the response of vegetation is not immediate. Rainfall increases soil water and atmospheric humidity reducing water stress in the plants. Similarly, in this research, mangroves did not respond immediately to rainfall, the mangrove greenness was weak and not significantly correlated with rainfall (Fig. 5), and mangrove greenness generally lagged behind rainfall (Fig. 4).

Regarding the phenological variables, the results revealed differences between VIs. One obvious contrast was the earlier dates of SOS, EOS and Max Green for NDWI compared to the rest of the vegetation indices (see Fig. 6). This asynchrony in phenological metrics may be explained by the sensitivity of the indices to different features of vegetation growth that may not necessarily occur simultaneously. The advanced SOS for NDWI observed in this study could be due to an increase in soil moisture before the development of new leaves as NDWI is not only sensitive to vegetation water content (Gao, 1996; Chen et al., 2005) but is also sensitive to soil moisture (Gao, 1996; Xiao et al., 2005a). Increases in NDWI proportional to soil moisture were observed in paddy fields before leaf on and proportional to leaf water content during leaf development (Xiao et al., 2002; De Alwis et al., 2007; Tornos et al., 2015). In addition, delayed phenological variables for NDWI were observed in the northwest of the Yucatan Peninsula, an area characterised by an arid and semi-arid climate (Fig. S1-S3). The ability of NDWI to vary proportionally according to soil moisture and canopy water stress makes it suitable to monitor mangrove forest water stress.

It is evident that EVI presents greater variability in the phenological metrics (Fig. 6). This variability may respond to the attributes of this vegetation index. EVI is a vegetation index primarily sensitive to canopy structural properties such as LAI, canopy cover and leaf structure (Gao et al., 2000).

629 Mangrove forests are heterogeneous landscapes composed of several species and individuals of
630 different age which may not respond uniformly to the environmental drivers. Therefore, the
631 mangrove's canopy structural properties vary spatially within a mangrove stand, and this structural
632 diversity is reflected in a greater variation in EVI phenological metrics. Another contrast was the
633 delayed SOS, Max Green and EOS dates for gNDVI. This delay could respond to mangrove leaf
634 development processes. Previous work suggests that gNDVI is more sensitive to mangrove leaf
635 chlorophyll concentration (Pastor-Guzman et al., 2015), a photosynthetic pigment that increases with
636 leaf age during the leaf development stage (Wang and Lin, 1999). The time to fully develop leaf
637 anatomy and photosynthetic pigments depends on the species and the time of the year that leaves are
638 born. Soto (1988), reported that new leaves of *A. germinans* reached their maximum size at between 4
639 to 6 months, whereas leaves from the genus *Rhizophora* reached their maximum mass, area and
640 chlorophyll concentration in 3 to 4 months (Wang and Lin, 1999; Mehlig, 2001; Sharma et al., 2014).
641 Therefore, it could be suggested that the delay in gNDVI phenological variables could be due to its
642 sensitivity to canopy chlorophyll content.
643 With respect to the drivers of mangrove forest phenology, our results revealed that sites receiving a
644 greater amount of rainfall between January and March experience earlier SOS and Max Green (Fig.
645 11 and Fig. S27-S28). The geology of the Yucatan Peninsula prevents the formation of rivers due to
646 the karstic permeable soil. Thus, fresh water contributions from runoff and rivers are practically non-
647 existent (Perry et al., 1995). The mangrove forest in the region receives fresh water inputs mainly
648 from rainfall and ground water discharges via springs when the aquifer recharge is greatest. This fresh
649 water is characterized by high inorganic nitrogen content, silicates and low particulate matter
650 (Herrera-Silveira, 1994; Herrera-Silveira et al., 1999). Given that milder salinity and greater
651 availability of nutrients leads to more favourable conditions for mangrove growth, it is reasonable to
652 speculate that cumulative rainfall plays an important role in mangrove phenology.
653 The results obtained in this research serve as a reference for future studies addressing long-term
654 phenological changes in the mangrove forest of the Yucatan Peninsula. Nevertheless, there are some
655 limitations that need to be taken into account. For example, the study focused on mangrove as a single
656 cover type; however, in reality the mangrove forest is not a homogeneous landscape but a complex

mosaic, a fragmented landscape that in many cases includes individuals of different ages, heights, open areas, and gaps with water ponds. Although the four mangrove species are dominant, in some areas there may be other communities embedded in the mangrove matrix such as grassland (Batllori-Sampedro and Febles-Patrón, 2007). Therefore, at 500 m spatial resolution the phenological pattern could be masked. Additional analyses showed that the mangrove forest phenology is clearly distinguished from that of terrestrial vegetation but it resembles that of surrounding flooded land cover types (Fig. S36-S37). In order to control for this source of uncertainty in this research we used only pixels that had more than 60% mangrove cover. Further examination revealed that the difference in the timing of SOS is marginal with a mangrove cover between 60% and 80% per MODIS pixel. At this coverage, it is assumed that the mangrove forest dominates the reflectance signal, supporting the use of this threshold. However, as the percentage of mangrove increases above 80% the SOS median shifts towards later DOY for about one month, suggesting pure mangrove stands may have delayed response to the environmental drivers (Fig. S29-S35). Another potential source of uncertainty can be the mismatch in the temporal and spatial resolution between the *in situ* data and the MODIS data. *In situ* data were collected monthly while MODIS data were 8-day composites; further, the sampling plots are not be evenly distributed within the MODIS pixel footprint. These sources of error could be minimized by adopting a sampling method designed to validate remote sensing observations (Elmendorf et al., 2016). Further, it should also be noted that other factors exist that may affect the seasonal dynamics of the vegetation indices on the mangrove forest such as clouds and aerosols. To reduce this source of potential errors, the QA MODIS layer was used to include only pixels with the highest quality.

5. Conclusion

This paper based on the Yucatan Peninsula is the first phenological characterisation of a mangrove forest using remote sensing data. The study used 15-year time-series of four vegetation indices computed from MODIS surface reflectance and the phenology was compared with climatic variables, salinity and litterfall. The DFT algorithm was used to smooth the time-series and four phenological variables were estimated: SOS, EOS, Max Green and LOS. The results revealed clear seasonality in mangrove forest greenness. Periods of lower greenness were typically associated with the dry season while periods of maximum greenness were associated with the months following maximum rainfall. The timing of the phenological variables differs depending on the vegetation index employed. In general, NDWI showed advanced phenological parameters whereas gNDVI showed delayed dates. SOS ranged between DOY 144 (late dry season) and DOY 220 (rainy season) while the EOS occurred between DOY 104 (mid-dry season) to DOY 160 (early rainy season). The length of the growing season ranged between 228 and 264 days. Interestingly, sites receiving a greater amount of rainfall between January and March have an advanced SOS and Max Green. These results show the potential of MODIS to monitor mangrove phenology at 500 m spatial resolution. MODIS constitutes a cost-effective tool to monitor temporal variation in mangroves as data are freely available at fine temporal resolution. The phenological calendar maps obtained are up-to-date and represent a reference for future research and the length of the time-series processed gives robustness to the phenological parameters. It is acknowledged, however, that the MODIS phenology product could be used in future studies if the tools or expertise required for the analysis are not available, or if the time available for fitting is limited. The results have implications for understanding mangrove forest dynamics at the landscape scale, and provide the potential to monitor biophysical variables such as water stress and canopy chlorophyll and their link to climatic variables at the global scale; information that could be used as input to bio-geochemical models. Finally, this study highlights the need to continue the long-term *in situ* data collection network in the mangrove forest.

6. Acknowledgements

The MOD09A1 data product was retrieved from the online Data Pool, courtesy of the NASA Land Processes Distributed Active Archive Center (LP DAAC), USGS/Earth Resources Observation and Science (EROS) Center, Sioux Falls, South Dakota. Special thanks to CONABIO for providing the *in situ* data to validate satellite observations and to the Mexican Council of Science and Technology (CONACYT) for the scholarship no. 311831 for JPG. Finally the authors thank the anonymous reviewers for the constructive criticism to improve the quality of the manuscript.

7. References

Adole, T., Dash, J., Atkinson, P.M., 2016. A systematic review of vegetation phenology in Africa. Ecol. Inform. 34, 117–128. doi:10.1016/j.ecoinf.2016.05.004

Alongi, D.M., 2016. Mangroves, in: Kennish, M.J. (Ed.), Encyclopedia of Estuaries. Springer Netherlands, Dordrecht, pp. 393–404.

Agraz-Hernández, C.M., García-Zaragoza, C., Iriarte-Vivar, S., Flores-Verdugo, F.J., Moreno-Casasola, P., 2011. Forest structure, productivity and species phenology of mangroves in the La Mancha lagoon in the Atlantic coast of Mexico. Wetl. Ecol. Manag. 19, 273–293. doi:10.1007/s11273-011-9216-4

Aké-Castillo, J.A., Vázquez, G., López-Portillo, J., 2006. Litterfall and Decomposition of Rhizophora mangle L. in a Coastal Lagoon in the Southern Gulf of Mexico. Hydrobiologia 559, 101–111. doi:10.1007/s10750-005-0959-x

Akmar, N.Z., Juliana, W.A.W., 2012. Reproductive phenology of two Rhizophora species in Sungai Pulai forest reserve, Johor, Malaysia. Malays. Appl. Biol. 41, 11–21.

Arreola-Lizárraga, J.A., Flores-Verdugo, F.J., Ortega-Rubio, A., 2004. Structure and litterfall of an arid mangrove stand on the Gulf of California, Mexico. Aquat. Bot. 79, 137–143. doi:10.1016/j.aquabot.2004.01.012

Atkinson, P.M., Jeganathan, C., Dash, J., Atzberger, C., 2012. Inter-comparison of four models for smoothing satellite sensor time-series data to estimate vegetation phenology. Remote Sens. Environ. 123, 400–417. doi:10.1016/j.rse.2012.04.001

Barr, J.G., Engel, V., Fuentes, J.D., Zieman, J.C., O'Halloran, T.L., Smith, T.J., Anderson, G.H., 2010. Controls on mangrove forest-atmosphere carbon dioxide exchanges in western Everglades National Park. J. Geophys. Res. 115. doi:10.1029/2009JG001186

738 Batllori-Sampedro, E., Febles-Patrón, J.L., 2007. Límites máximos permisibles para el
739 aprovechamiento del ecosistema de manglar. Gac. Ecológica INE-SEMARNAT Mex. 82, 5–23.

740 Bouillon, S., Borges, A.V., Castañeda-Moya, E., Diele, K., Dittmar, T., Duke, N.C., Kristensen, E.,
741 Lee, S.Y., Marchand, C., Middelburg, J.J., Rivera-Monroy, V.H., Smith, T.J., Twilley, R.R., 2008.
742 Mangrove production and carbon sinks: A revision of global budget estimates: GLOBAL
743 MANGROVE CARBON BUDGETS. Glob. Biogeochem. Cycles 22, n/a-n/a.
744 doi:10.1029/2007GB003052

745 Castañeda-Moya, E., Twilley, R.R., Rivera-Monroy, V.H., 2013. Allocation of biomass and net
746 primary productivity of mangrove forests along environmental gradients in the Florida Coastal
747 Everglades, USA. For. Ecol. Manag. 307, 226–241. doi:10.1016/j.foreco.2013.07.011

748 Cerón-Souza, I., Turner, B.L., Winter, K., Medina, E., Bermingham, E., Feliner, G.N., 2014.
749 Reproductive phenology and physiological traits in the red mangrove hybrid complex (Rhizophora
750 mangle and R. racemosa) across a natural gradient of nutrients and salinity. Plant Ecol. 215, 481–493.
751 doi:10.1007/s11258-014-0315-1

752 Chave, J., Navarrete, D., Almeida, S., Alvarez, E., Aragão, L.E., Bonal, D., Châtelet, P., Silva-Espejo,
753 J.E., Goret, J.-Y., Hildebrand, P. von, others, 2010. Regional and seasonal patterns of litterfall in
754 tropical South America. Biogeosciences 7, 43–55.

755 Chen, D., Huang, J., Jackson, T.J., 2005. Vegetation water content estimation for corn and soybeans
756 using spectral indices derived from MODIS near- and short-wave infrared bands. Remote Sens.
757 Environ. 98, 225–236. doi:10.1016/j.rse.2005.07.008

758 Cleland, E., Chuine, I., Menzel, A., Mooney, H., Schwartz, M., 2007. Shifting plant phenology in
759 response to global change. Trends Ecol. Evol. 22, 357–365. doi:10.1016/j.tree.2007.04.003

760 CONABIO, 2009. Manglares de Mexico: Estension y distribucion., 2nd ed. Comisión Nacional para
761 el Conocimiento y Uso de la Biodiversidad. México.

762 CONABIO, (2013). 'Mapa de uso del suelo y vegetación de la zona costera asociada a los manglares,
763 Region Península de Yucatán (2010).', escala: 1:50000. edición: 1. Comisión Nacional para el
764 Conocimiento y Uso de la Biodiversidad. Proyecto: GQ004, Los manglares de México: Estado actual
765 y establecimiento de un programa de monitoreo a largo plazo: 2da y 3era etapas.. México, DF.

766 Coupland, G.T., Paling, E.I., McGuinness, K.A., 2005. Vegetative and reproductive phenologies of
767 four mangrove species from northern Australia. Aust. J. Bot. 53, 109–117. doi:10.1071/bt04066

768 Dannenberg, M.P., Song, C., Hwang, T., Wise, E.K., 2015. Empirical evidence of El Niño–Southern
769 Oscillation influence on land surface phenology and productivity in the western United States.
770 Remote Sens. Environ. 159, 167–180. doi:10.1016/j.rse.2014.11.026

771 Dash, J., Jeganathan, C., Atkinson, P.M., 2010. The use of MERIS Terrestrial Chlorophyll Index to
772 study spatio-temporal variation in vegetation phenology over India. Remote Sens. Environ. 114,
773 1388–1402. doi:10.1016/j.rse.2010.01.021

774 Day, J.W.J., Conner, W.H., Ley-Lou, F., Day, R.H., Machado-Navarro, A., 1987. The productivity
775 and composition of mangrove forests, Laguna de Terminos, Mexico. Aquat. Bot. 27, 267–284.

776 Day Jr., J.W., Coronado-Molina, C., Vera-Herrera, F.R., Twilley, R., Rivera-Monroy, V.H., Alvarez-
777 Guillen, H., Day, R., Conner, W., 1996. A 7 year record of above-ground net primary production in a
778 southeastern Mexican mangrove forest. Aquat. Bot. 55, 39–60. doi:10.1016/0304-3770(96)01063-7

779 De Alwis, D.A., Easton, Z.M., Dahlke, H.E., Philpot, W.D., Steenhuis, T.S., 2007. Unsupervised
780 classification of saturated areas using a time series of remotely sensed images. Hydrol. Earth Syst.
781 Sci. Discuss. 11, 1609–1620.

782 Donato, D.C., Kauffman, J.B., Murdiyarso, D., Kurnianto, S., Stidham, M., Kanninen, M., 2011.
783 Mangroves among the most carbon-rich forests in the tropics. Nat. Geosci. 4, 293–297.
784 doi:10.1038/ngeo1123

785 Duke, N.C., 1990. Phenological Trends with Latitude in the Mangrove Tree Avicennia Marina. J.
786 Ecol. 78, 113. doi:10.2307/2261040

787 Elmendorf, S.C., Jones, K.D., Cook, B.I., Diez, J.M., Enquist, C.A.F., Hufft, R.A., Jones, M.O.,
788 Mazer, S.J., Miller-Rushing, A.J., Moore, D.J.P., Schwartz, M.D., Weltzin, J.F., 2016. The plant
789 phenology monitoring design for The National Ecological Observatory Network. Ecosphere 7.
790 doi:10.1002/ecs2.1303

791 Fernandes, M.E., 1999. Phenological patterns of Rhizophora L., Avicennia L. and Laguncularia
792 Gaertn. f. in Amazonian mangrove swamps, in: Diversity and Function in Mangrove Ecosystems.
793 Springer, pp. 53–62.

794 Fitter, A.H., Fitter, R.S.R., 2002. Rapid changes in flowering time in British plants. Science 296,
795 1689–1691.

796 Gao, B., 1996. NDWI—A normalized difference water index for remote sensing of vegetation liquid
797 water from space. Remote Sens. Environ. 58, 257–266. doi:10.1016/S0034-4257(96)00067-3

798 Gao, X., Huete, A.R., Ni, W., Miura, T., 2000. Optical–biophysical relationships of vegetation spectra
799 without background contamination. Remote Sens. Environ. 74, 609–620.

800 Geerken, R.A., 2009. An algorithm to classify and monitor seasonal variations in vegetation
801 phenologies and their inter-annual change. ISPRS J. Photogramm. Remote Sens. 64, 422–431.
802 doi:10.1016/j.isprsjprs.2009.03.001

803 Gill, A.M., Tomlinson, P.B., 1971. Studies on the Growth of Red Mangrove (Rhizophora mangle L.)
804 3. Phenology of the Shoot. Biotropica 3, 109. doi:10.2307/2989815

805 Gitelson, A.A., Kaufman, Y.J., Merzlyak, M.N., 1996. Use of a green channel in remote sensing of
806 global vegetation from EOS-MODIS. Remote Sens. Environ. 58, 289–298. doi:10.1016/S0034-
807 4257(96)00072-7

Hasegawa, P.M., Bressan, R.A., Zhu, J.-K., Bohnert, H.J., 2000. Plant cellular and molecular responses to high salinity. Annu. Rev. Plant Biol. 51, 463–499.

Herrera-Silveira, J., Morales-Ojeda, S., 2010. Subtropical Karstic Coastal Lagoon Assessment, Southeast Mexico, in: Coastal Lagoons, Marine Science. CRC Press, pp. 307–333. doi:10.1201/EBK1420088304-c13

Herrera-Silveira, J.A., 1994. Spatial Heterogeneity and Seasonal Patterns in a Tropical Coastal Lagoon. J. Coast. Res. 10.

Herrera-Silveira, J.A., R., J.R., J., A.Z., 1999. Overview and characterization of the hydrology and primary producer communities of selected coastal lagoons of Yucatán, México. Aquat. Ecosyst. Health Manag. 1, 353–372. doi:10.1080/14634989808656930

Herrera-Silveira, Teutli-Hernández, C., Zaldívar-Jiménez, A., Pérez-Ceballos, R., Cortés-Balán, O., Osorio-Moreno, I., Ramírez-Ramírez, J., Caamal-Sosa, J., Andueza-Briceño, T.T., Torres, R., Hernández-Aranda, H., 2014. Programa regional para la caracterización y el monitoreo de ecosistemas de manglar del Golfo de México y Caribe Mexicano: Península de Yucatán (Informe final SNIB-CONABIO No. FN009). Centro de Investigación y de Estudios Avanzados-Mérida, México D. F.

Hoque, M.M., Mustafa Kamal, A.H., Idris, M.H., Haruna Ahmed, O., Rafiqul Hoque, A.T.M., Masum Billah, M., 2015. Litterfall production in a tropical mangrove of Sarawak, Malaysia. Zool. Ecol. 25, 157–165. doi:10.1080/21658005.2015.1016758

Huete, A., Didan, K., Miura, T., Rodriguez, E.P., Gao, X., Ferreira, L.G., 2002. Overview of the radiometric and biophysical performance of the MODIS vegetation indices. Remote Sens. Environ. 83, 195–213.

Jakubauskas, M.E., Legates, D.R., Kastens, J.H., 2001. Harmonic analysis of time-series AVHRR NDVI data 461–470.

832 Jeganathan, C., Dash, J., Atkinson, P.M., 2014. Remotely sensed trends in the phenology of northern
833 high latitude terrestrial vegetation, controlling for land cover change and vegetation type. Remote
834 Sens. Environ. 143, 154–170. doi:10.1016/j.rse.2013.11.020

835 Jeganathan, C., Dash, J., Atkinson, P.M., 2010a. Characterising the spatial pattern of phenology for
836 the tropical vegetation of India using multi-temporal MERIS chlorophyll data. Landsc. Ecol. 25,
837 1125–1141. doi:10.1007/s10980-010-9490-1

838 Jönsson, P., Eklundh, L., 2004. TIMESAT—a program for analyzing time-series of satellite sensor
839 data. Comput. Geosci. 30, 833–845. doi:10.1016/j.cageo.2004.05.006

840 Jönsson, P., Eklundh, L., 2002. Seasonality extraction by function fitting to time-series of satellite
841 sensor data. IEEE Trans. Geosci. Remote Sens. 40, 1824–1832. doi:10.1109/TGRS.2002.802519

842 Julien, Y., Sobrino, J.A., 2009. Global land surface phenology trends from GIMMS database. Int. J.
843 Remote Sens. 30, 3495–3513. doi:10.1080/01431160802562255

844 Kamruzzaman, M., Kamara, M., Sharma, S., Hagihara, A., 2016. Stand structure, phenology and
845 litterfall dynamics of a subtropical mangrove Bruguiera gymnorrhiza. J. For. Res. 27, 513–523.
846 doi:10.1007/s11676-015-0195-9

847 Klosterman, S.T., Hufkens, K., Gray, J.M., Melaas, E., Sonnentag, O., Lavine, I., Mitchell, L.,
848 Norman, R., Friedl, M.A., Richardson, A.D., 2014. Evaluating remote sensing of deciduous forest
849 phenology at multiple spatial scales using PhenoCam imagery. Biogeosciences 11, 4305–4320.
850 doi:10.5194/bg-11-4305-2014

851 Leach, G.J., Burgin, S., 1985. Litter production and seasonality of mangroves in Papua New Guinea.
852 Aquat. Bot. 23, 215–224. doi:10.1016/0304-3770(85)90067-1

853 Lopez-Portillo, J., Ezcurra, E., 1985. Litter Fall of Avicennia germinans L. in a One-Year Cycle in a
854 Mudflat at the Laguna de Mecoacan, Tabasco, Mexico. Biotropica 17, 186. doi:10.2307/2388215

855 Medina, E., 1999. Mangrove physiology: the challenge of salt, heat, and light stress under recurrent
856 flooding. Ecosistemas Mangl. En América Trop. 10–126.

857 Mehlig, U., 2006. Phenology of the red mangrove, Rhizophora mangle L., in the Caeté Estuary, Pará,
858 equatorial Brazil. Aquat. Bot. 84, 158–164. doi:10.1016/j.aquabot.2005.09.007

859 Mehlig, U., 2001. Aspects of tree primary production in an equatorial mangrove forest in Brazil. ZMT
860 Contribution 14. Center for Marine Tropical Ecology (ZMT), Bremen, Germany.

861 Mizunuma, T., Wilkinson, M., L. Eaton, E., Mencuccini, M., I. L. Morison, J., Grace, J., 2013. The
862 relationship between carbon dioxide uptake and canopy colour from two camera systems in a
863 deciduous forest in southern England. Funct. Ecol. 27, 196–207. doi:10.1111/1365-2435.12026

864 Moody, A., Johnson, D.M., 2001. Land-surface phenologies from AVHRR using the discrete Fourier
865 transform. Remote Sens. Environ. 75, 305–323.

866 Moulin, S., Kergoat, L., Viovy, N., Dedieu, G., 1997. Global-scale assessment of vegetation
867 phenology using NOAA/AVHRR satellite measurements. J. Clim. 10, 1154–1170.

868 Njoku, E.G. (Ed.), 2014. Encyclopedia of Remote Sensing, Encyclopedia of Earth Sciences Series.
869 Springer New York, New York, NY.

870 Pastor-Guzman, J., Atkinson, P., Dash, J., Rioja-Nieto, R., 2015. Spatiotemporal Variation in
871 Mangrove Chlorophyll Concentration Using Landsat 8. Remote Sens. 7, 14530–14558.
872 doi:10.3390/rs71114530

873 Perry, E., Marin, L., McClain, J., Velazquez, G., 1995. Ring of cenotes (sinkholes), northwest
874 Yucatan, Mexico: its hydrogeologic characteristics and possible association with the Chicxulub
875 impact crater. Geology 23, 17–20.

876 Pope, K.O., Rejmankova, E., Paris, J.F., Woodruff, R., 1997. Detecting seasonal flooding cycles in
877 marshes of the Yucatan Peninsula with SIR-C polarimetric radar imagery. Remote Sens. Environ. 59,
878 157–166. doi:10.1016/s0034-4257(96)00151-4

R Core Team, 2015. R: A Language and Environment for Statistical Computing. R Foundation for Statistical Computing., Vienna, Austria.

Rajkaran, A., Adams, J., 2007. Mangrove litter production and organic carbon pools in the Mngazana Estuary, South Africa. Afr. J. Aquat. Sci. 32, 17–25. doi:10.2989/AJAS.2007.32.1.3.140

Reed, B.C., Brown, J.F., VanderZee, D., Loveland, T.R., Merchant, J.W., Ohlen, D.O., 1994b. Measuring phenological variability from satellite imagery. J. Veg. Sci. 5, 703–714.

Reed, B.C., Schwartz, M.D., Xiao, X., 2009. Remote Sensing Phenology, in: Noormets, A. (Ed.), Phenology of Ecosystem Processes. Springer New York, New York, NY, pp. 231–246.

Richardson, A.D., Jenkins, J.P., Braswell, B.H., Hollinger, D.Y., Ollinger, S.V., Smith, M.-L., 2007. Use of digital webcam images to track spring green-up in a deciduous broadleaf forest. Oecologia 152, 323–334. doi:10.1007/s00442-006-0657-z

Richardson, A.D., Keenan, T.F., Migliavacca, M., Ryu, Y., Sonnentag, O., Toomey, M., 2013. Climate change, phenology, and phenological control of vegetation feedbacks to the climate system. Agric. For. Meteorol. 169, 156–173. doi:10.1016/j.agrformet.2012.09.012

Rodriguez-Galiano, V., Dash, J., Atkinson, P., 2015a. Characterising the Land Surface Phenology of Europe Using Decadal MERIS Data. Remote Sens. 7, 9390–9409. doi:10.3390/rs70709390

Rodriguez-Galiano, V.F., Dash, J., Atkinson, P.M., 2015b. Intercomparison of satellite sensor land surface phenology and ground phenology in Europe: Inter-annual comparison and modelling. Geophys. Res. Lett. 42, 2253–2260. doi:10.1002/2015GL063586

Roerink, G.J., Menenti, M., Verhoef, W., 2000. Reconstructing cloudfree NDVI composites using Fourier analysis of time series. Int. J. Remote Sens. 21, 1911–1917. doi:10.1080/014311600209814

Roger Orellana, Celene Espadas, Cecilia Conde, Carlos Gay, CICY, UNAM, CONACYT, SEDUMA-Gobiernodel Estado de Yucatán, SIDETEY, ONU-PNUD, 2009. Atlas. Escenarios de cambio climático en la Península de Yucatán. Mérida, Yucatán.

903 Sharma, S., Hoque, A.T.M.R., Analuddin, K., Hagihara, A., 2014. A model of seasonal foliage
904 dynamics of the subtropical mangrove species Rhizophora stylosa Griff. growing at the northern limit
905 of its distribution. For. Ecosyst. 1, 1–11.

906 Slim, F.J., Gwada, P.M., Kodjo, M., Hemminga, M.A., 1996. Biomass and litterfall of Ceriops tagal
907 and Rhizophora mucronata in the mangrove forest of Gazi Bay, Kenya. Mar. Freshw. Res. 47, 999–
908 1007.

909 Song, C., White, B.L., Heumann, B.W., 2011. Hyperspectral remote sensing of salinity stress on red (
910 Rhizophora mangle) and white (Laguncularia racemosa) mangroves on Galapagos Islands. Remote
911 Sens. Lett. 2, 221–230. doi:10.1080/01431161.2010.514305

912 Soto, R., 1988. Geometry, biomass allocation and leaf life-span of Avicennia germinans
913 L.(Avicenniaceae) along a salinity gradient in Salinas, Puntarenas, Costa Rica. Rev. Biol. Trop. 36,
914 309–324.

915 Stöckli, R., Vidale, P.L., 2004. European plant phenology and climate as seen in a 20-year AVHRR
916 land-surface parameter dataset. Int. J. Remote Sens. 25, 3303–3330.
917 doi:10.1080/01431160310001618149

918 Sukardjo, S., Alongi, D.M., Kusmana, C., 2013. Rapid litter production and accumulation in Bornean
919 mangrove forests. Ecosphere 4, 1–7. doi:10.1890/ES13-00145.1

920 Tomlinson, P.B., 1995. The Botany of Mangroves. Cambridge University Press, Cambridge.

921 Tornos, L., Huesca, M., Dominguez, J.A., Moyano, M.C., Cicuendez, V., Recuero, L., Palacios-
922 Orueta, A., 2015. Assessment of MODIS spectral indices for determining rice paddy agricultural
923 practices and hydroperiod. ISPRS J. Photogramm. Remote Sens. 101, 110–124.
924 doi:10.1016/j.isprsjprs.2014.12.006

925 Twilley, R.R., Day, J.W., 1999. The productivity and nutrient cycling of mangrove ecosystem.
926 Ecosistemas Mangl. En América Trop. Inst. Ecol. AC México UICNORMA Costa Rica NOAANMFS
927 Silver Spring MD EUA P 127–151.

928 Upadhyay, V.P., Mishra, P.K., 2010. Phenology of mangroves tree species on Orissa coast, India.
929 Trop. Ecol. 51, 289–295.

930 Utrera-López, M.E., Moreno-Casasola, P., 2008. Mangrove litter dynamics in La Mancha Lagoon,
931 Veracruz, Mexico. Wetl. Ecol. Manag. 16, 11–22. doi:10.1007/s11273-007-9042-x

932 Wafar, S., Untawale, A.G., Wafar, M., 1997. Litter Fall and Energy Flux in a Mangrove Ecosystem.
933 Estuar. Coast. Shelf Sci. 44, 111–124. doi:10.1006/ecss.1996.0152

934 Wagenseil, H., Samimi, C., 2006. Assessing spatio-temporal variations in plant phenology using
935 Fourier analysis on NDVI time series: results from a dry savannah environment in Namibia. Int. J.
936 Remote Sens. 27, 3455–3471. doi:10.1080/01431160600639743

937 Wang, W., Lin, P., 1999. Transfer of salt and nutrients in Bruguiera gymnorrhiza leaves during
938 development and senescence. Mangroves Salt Marshes 3, 1–7.

939 White, M.A., Running, S.W. and Thornton, P.E. (1999) The impact of growing-season length
940 variability on carbon assimilation and evapotranspiration over 88 years in the eastern US deciduous
941 forest. Int. J. Biometeorol. 42, 139–145.

942 White, M.A., Thornton, P.E. and Running, S.W. (1997) A continental phenology model for
943 monitoring vegetation responses to interannual climatic variability. Global Biogeochem. Cycles 11,
944 217–234.

945 Xiao, X., Boles, S., Frolking, S., Salas, W., Moore, B., Li, C., He, L., Zhao, R., 2002. Observation of
946 flooding and rice transplanting of paddy rice fields at the site to landscape scales in China using
947 VEGETATION sensor data. Int. J. Remote Sens. 23, 3009–3022. doi:10.1080/01431160110107734

948 Xiao, X., Boles, S., Liu, J., Zhuang, D., Frolking, S., Li, C., Salas, W., Moore, B., 2005a. Mapping
949 paddy rice agriculture in southern China using multi-temporal MODIS images. Remote Sens.
950 Environ. 95, 480–492. doi:10.1016/j.rse.2004.12.009

951 Xiao, X., Zhang, Q., Saleska, S., Hutyra, L., De Camargo, P., Wofsy, S., Frolking, S., Boles, S.,
952 Keller, M., Moore, B., 2005b. Satellite-based modeling of gross primary production in a seasonally
953 moist tropical evergreen forest. Remote Sens. Environ. 94, 105–122. doi:10.1016/j.rse.2004.08.015

954 Xu, L., Myneni, R.B., Chapin III, F.S., Callaghan, T.V., Pinzon, J.E., Tucker, C.J., Zhu, Z., Bi, J.,
955 Ciais, P., Tømmervik, H., Euskirchen, E.S., Forbes, B.C., Piao, S.L., Anderson, B.T., Ganguly, S.,
956 Nemani, R.R., Goetz, S.J., Beck, P.S.A., Bunn, A.G., Cao, C., Stroeve, J.C., 2013. Temperature and
957 vegetation seasonality diminishment over northern lands. Nat. Clim. Change.
958 doi:10.1038/nclimate1836

959 Zaldivar-Jimenez, A., Herrera-Silveira, J., Coronado-Molina, C., Alonzo-Parra, D., 2004. Estructura y
960 productividad de los manglares en la Reserva de la Biosfera Ria Celestun, Yucatan, Mexico. Madera
961 Bosques 10, 25–35.

962 Zhang, H., Yuan, W., Dong, W., Liu, S., 2014. Seasonal patterns of litterfall in forest ecosystem
963 worldwide. Ecol. Complex. 20, 240–247. doi:10.1016/j.ecocom.2014.01.003

964 Zhang, X., Friedl, M.A., Schaaf, C.B., 2006. Global vegetation phenology from Moderate Resolution
965 Imaging Spectroradiometer (MODIS): Evaluation of global patterns and comparison with in situ
966 measurements. J. Geophys. Res. 111. doi:10.1029/2006JG000217

967 Zhang, X., Friedl, M.A., Schaaf, C.B., Strahler, A.H., Hodges, J.C., Gao, F., Reed, B.C., Huete, A.,
968 2003. Monitoring vegetation phenology using MODIS. Remote Sens. Environ. 84, 471–475.

969 Zheng, W., Wang, W., Lin, P., 1999. Dynamics of element contents during the development of
970 hypocotyls and leaves of certain mangrove species. J. Exp. Mar. Biol. Ecol. 233, 247–257.
971 doi:10.1016/S0022-0981(98)00131-2